Korean J. Chem. Eng., 40(4), 740-753 (2023)
DOI: 10.1007/s11814-022-1331-9

pISSN: 0256-1115
eISSN: 1975-7220

Techno-economic analysis of CO_2/steam co-electrolysis process and synfuel production process coupled with steel manufacturing process

Gi Hoon Hong*,‡, Juwon Lee,‡, Youngtak Cho***, and Sungwon Hwang**,***,†**

*Plant Process Development Center, Institute for Advanced Engineering, Yongin-si 17180, Republic of Korea
**Department of Chemistry and Chemical Engineering, Education and Research Center for Smart Energy and Materials, Inha University, Incheon 22212, Republic of Korea
***Department of Smart Digital Engineering, Inha University, Incheon 22212, Republic of Korea
(*Received 25 May 2022 • Revised 3 October 2022 • Accepted 31 October 2022*)

Abstract−Over the past few decades, reducing CO_2 emissions has attracted attention at an industrial level worldwide. This study focuses on utilizing both the byproduct gas, including CO_2, and waste heat produced from the steel-making process to produce synthetic fuel by integrating solid oxide electrolyzer cell (SOEC) technology with downstream Fischer-Tropsch and hydrocracking processes. CO_2 can be collected from the byproduct gas and used as a feed for the SOEC, and waste heat from the steel-making process can be utilized as the main heat source for operation of the SOEC at high temperatures and to generate electrical power through heat recovery and steam generation (HRSG) as an energy source for the SOEC. The syngas (H_2 and CO) produced from the SOEC is then converted to synthetic oil through the FT process, and the yield of the synthetic oil is increased via the hydrocracking process by converting heavy oil to lighter fractions. The entire process was modeled using Aspen HYSYS software, and pinch technology was adopted to maximize the energy efficiency of the process. As a result, CO_2 release was reduced by 452 tons/day and syngas was produced by 336.8 tons/day. The syngas produced was then converted to synthetic oil (306.7 tons/day) and light gas (44.24 tons/day). Economic assessment was completed based on the discounted cash flow method for two cases: electricity tariffs and new renewable energy prices. When the electricity tariff is implemented, profit is achieved in seven years, whereas the system becomes profitable in four years when newly regenerated surplus energy is utilized. If the price of renewable energy is reduced, profits may be achieved earlier.

Keywords: CO_2, SOEC, Fischer-Tropsch, Economic Assessment, Hydrocracking

INTRODUCTION

Reducing greenhouse gas emissions is a global requirement imposed in the follow-up measures stipulated in the climate agreement of 21st Conference of the Parties (COP21) and 25th Conference of the Parties (COP25). This requirement to achieve greenhouse gas reduction targets imposes a significant burden on the cement, steel, and power industries [1]. For this reason, there has been increasing interest in developing a chemical CO_2 conversion system wherein various CO_2 capture technologies are used to convert CO_2 to fuel form. For example, a large amount of CO_2 is produced from the steel-making process, which uses a large amount of coke and carbon raw material to reduce pig iron. As a CO_2 conversion technology, CO_2 co-electrolysis has received much attention because it produces synthetic gas electrochemically using CO_2 and steam as raw materials. The co-electrolysis system operates at high temperatures and is the reverse of the solid oxide fuel cell (SOFC) reaction. From a solid oxide electrolysis cell (SOEC) stack with a power supply, CO_2/steam is electrolyzed into synthetic gas (syngas) comprising CO and H_2. The efficiency of the system is highly dependent on the operating temperature of the SOEC stack, which generally exceeds 800 °C. Dieterich et al. reviewed the conversion of H_2 and CO_2 to methanol, DME, or Fischer-Tropsch (F-T) fuel through a power-to-liquid (PtL) process [2]. Lee et al. developed a process model for producing olefins and supplying power using off-gas from steelworks, and performed economic analysis through disconnected cash flow analysis [3]. Xi et al. developed a low-carbon steelworks gas utilization system that integrates methanol production-based carbon utilization and renewable power, and proposed the optimal operation scheduling based on meteorological and load conditions using artificial intelligence technology [4]. Gao et al. used Aspen Plus software to build a methanol production model using coke-oven gas (COG) and LDG, and studied the impact of the recycling rates on the technical and economic performance of the system [5]. Zeng et al. attempted to optimize the utilization of by-products, steam, and electricity from steel mills to reduce energy costs and CO_2 emissions [6].

de Ras et al. showed the importance of recycling and converting blast furnace (BF) waste gas and producing hydrogen using green electricity in an energy efficient and inexpensive process [7]. Czachor et al. constructed a model to generate hydrogen from COG and steam from a steel mill process using co-electrolysis, where they enhanced the reverse water-gas shift reaction by controlling the operating voltage [8]. Fu et al. developed a process model for producing synthetic gas through high-temperature co-electrolysis using

†To whom correspondence should be addressed.
E-mail: sungwon.hwang@inha.ac.kr
‡These authors contributed equally.

SOEC and synthetic fuel through F-T synthesis (FTS) and biomass-to-liquid (BTL) conversion [9]. O'Brien et al. conducted a parametric study of synthetic gas production by supplying the heat and power required to generate 300 MW of power through an SOEC. For this purpose, the waste heat from a nuclear reactor power plant was reused for power generation using a steam turbine [10]. Becker et al. modeled a process in which synthetic gas is produced through SOEC-based CO_2 and steam co-electrolysis, and synthetic fuel is generated through the FTS reaction. They performed a sensitivity analysis by considering the power consumption with varying SOEC operating pressure [11]. Salomone et al. used a serially operating internal combustion (SOIC) facility for water electrolysis using excess renewable energy sources (RES). They produced hydrogen and mixed it with CO_2 to produce synthetic natural gas via a methanation reaction. Finally, they performed a techno-economic analysis for the power-to-gas (P2G) system and derived the levelized cost of the product (LCOP) [12].

As illustrated in the above studies, waste gas recycling in steel mills has been extensively studied. Emphasis has been placed on finding solutions for reusing waste energy and achieving carbon reduction by adopting SOEC-based electrochemical technology. This study focuses on techno-economic analysis of the SOEC electrochemical process integrated with F-T and hydrocracking processes, where the waste heat and byproduct gas generated from the steel-making process are utilized. Aspen Energy Analyzer (ver.12.1) is used to apply the pinch technology to design heat exchanger networks to maximize heat recovery from waste heat. To model the individual processes, Aspen HYSYS (ver.11.0) is used to model the SOEC, F-T, and hydrocracking processes. The economic evaluation tool in Aspen HYSYS and the chemical engineering plant cost index (CEPCI) are used for the economic analysis and project validity evaluation.

PROCESS DESCRIPTION

Fig. 1 shows a block diagram of the overall process. Waste heat and byproduct gas are generated from the steel milling process, where the byproduct gas contains significant amounts of H_2, CO, and CO_2, among others. This gas is pretreated and separated via different adsorption units. CO_2 is used as the feed to the SOEC, while CO and H_2 are supplied to the F-T unit. The waste heat is used to produce steam, and a portion of it is used as a feed stream to the SOEC, whereas the remaining heat is used for either indirect heat transfer or generation of electricity through a steam turbine. In contrast, the remaining waste heat is directly used to increase the temperature of the feed streams (such as steam and CO_2) to the SOEC unit, where the operation temperature is ~900 °C. The SOEC consumes electricity to convert CO_2 and steam to H_2 and CO, which are fed to the F-T unit, while additional CO and H_2 are injected from the byproduct gas treatment unit. Through the F-T process, synthetic oil and gas are produced, and the downstream hydrocracking process converts heavy oils into lighter oils by cracking hydrocarbons. As a result, valuable products such as synthetic oil and gas can be produced from byproduct gas and waste heat by integrating the SOEC with F-T and hydrocracking units.

Waste heat and byproduct gas were utilized for producing synthetic oil and gas, as shown in Fig. 2. Waste heat was used in 16 heat exchangers, H_2 was obtained from COG, and CO_2 was obtained from blast furnace gas (BFG) and supplied to the SOEC. The amount of LDG was small, and only waste heat was recovered. H_2O was supplied to the SOEC in the form of hot steam generated by using the waste heat. The PSA H_2 process compresses the gas to 24.13 bar and its temperature is 37.7 °C. The PSA CO_2 process compresses the gas to 9.4 bar and its temperature is 25 °C. And both PSA CO_2 and PSA H_2 processes use two adsorption columns.

To implement the high-temperature co-electrolysis (HTCE) system, Aspen HYSYS was used to simulate the SOEC module, as shown in Fig. 3. For reference, the required amount of power was estimated based on Eqs. (1)-(8) by considering the amount of CO_2 and steam that are supplied to the reactor. Furthermore, because the RWGS reaction is promoted in the SOEC, a Gibbs reactor was used to present this reaction.

$$P_{total}=V_{cell}\cdot I_{total} \quad (1)$$

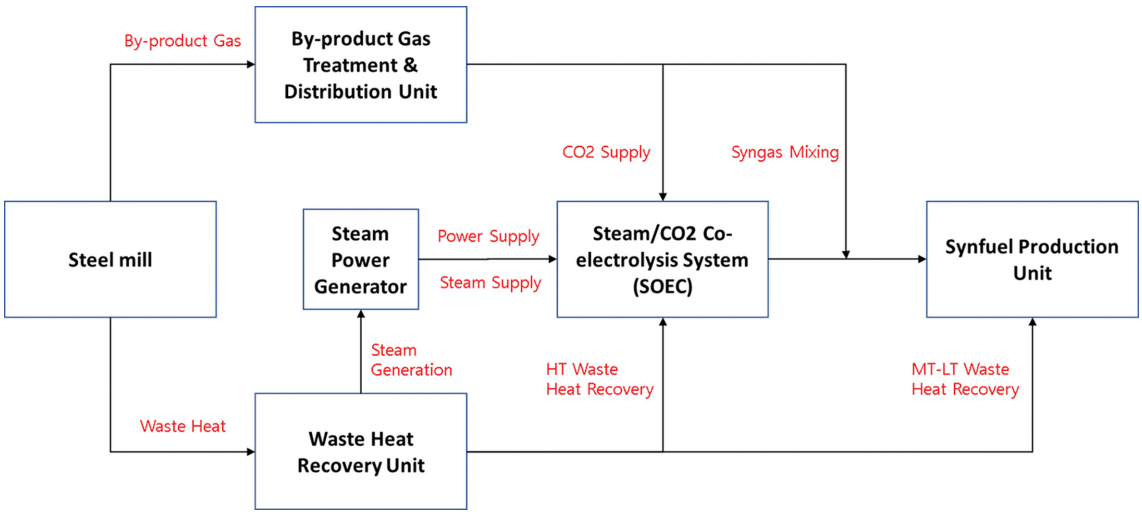

Fig. 1. Overall process flow.

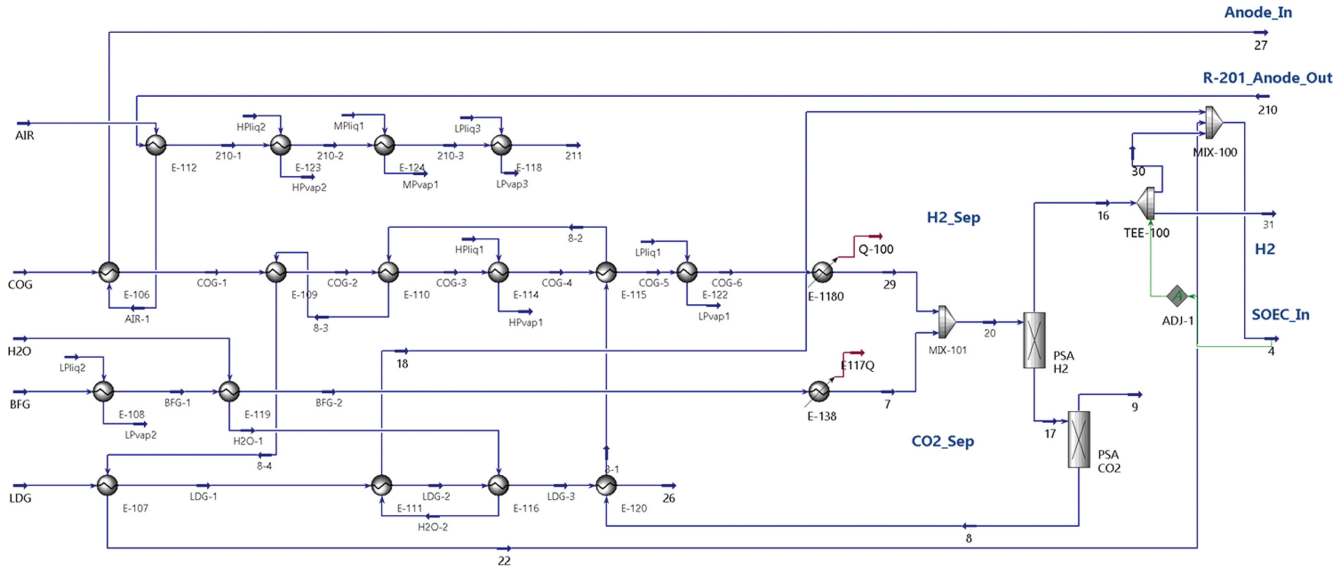

Fig. 2. Waste heat recovery unit from Aspen HYSYS.

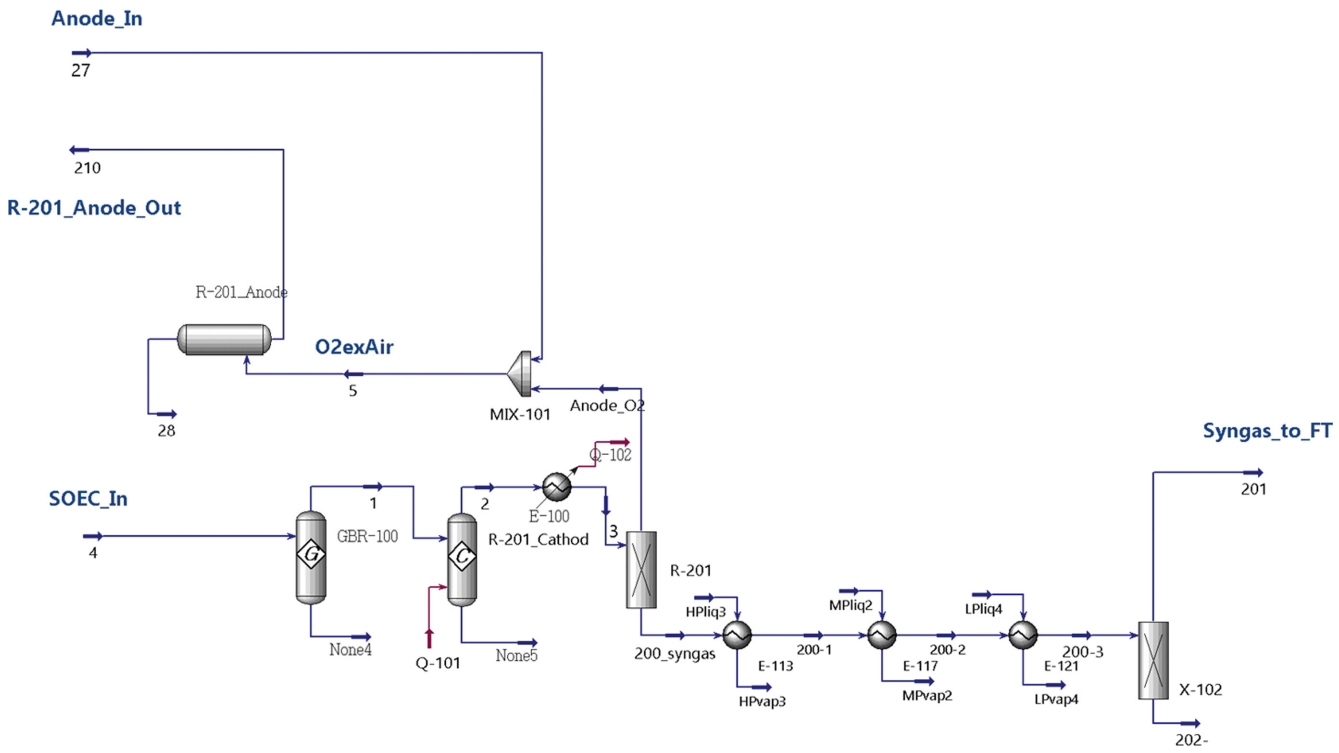

Fig. 3. Solid oxide electrolysis cell (SOEC) unit modeled in Aspen HYSYS.

$$I_{total}=N_{cell}\cdot I_{cell} \quad (2)$$

$$I_{cell}=A_{cell}\cdot j \quad (3)$$

$$\dot{M}_{H_2,\,CO\,prod}=\dot{M}_{H_2O,\,CO_2\,electrol}=\frac{I_{total}}{2\cdot F} \quad (4)$$

$$I_{total}=\dot{M}_{H_2,\,CO\,prod}\cdot 2\cdot F \quad (5)$$

$$V_{cell}=\frac{\Delta G_{H_2,\,CO}}{2\cdot F}-\frac{RT}{2\cdot F}\ln\frac{[p_{H_2,\,CO}]}{p_{H_2O,\,CO_2}} \quad (6)$$

$$\Delta E_{decomp}=\dot{M}\cdot\Delta H_{H_2,\,CO} \quad (7)$$

$$Q_{SOEC}=P_{total}-\Delta E_{decomp} \quad (8)$$

FTS utilizing the syngas obtained from the SOEC is shown in Fig. 4 and 5. Syngas multi-stage compression proceeds because of the FTS conditions, and the products of the F-T reaction (FTR) are separated by passing through hot, high-pressure separators (HHPSs), cold high-pressure separators (CHPSs), and cold low-pressure separators (CLPSs). These heavy materials are cracked to form mate-

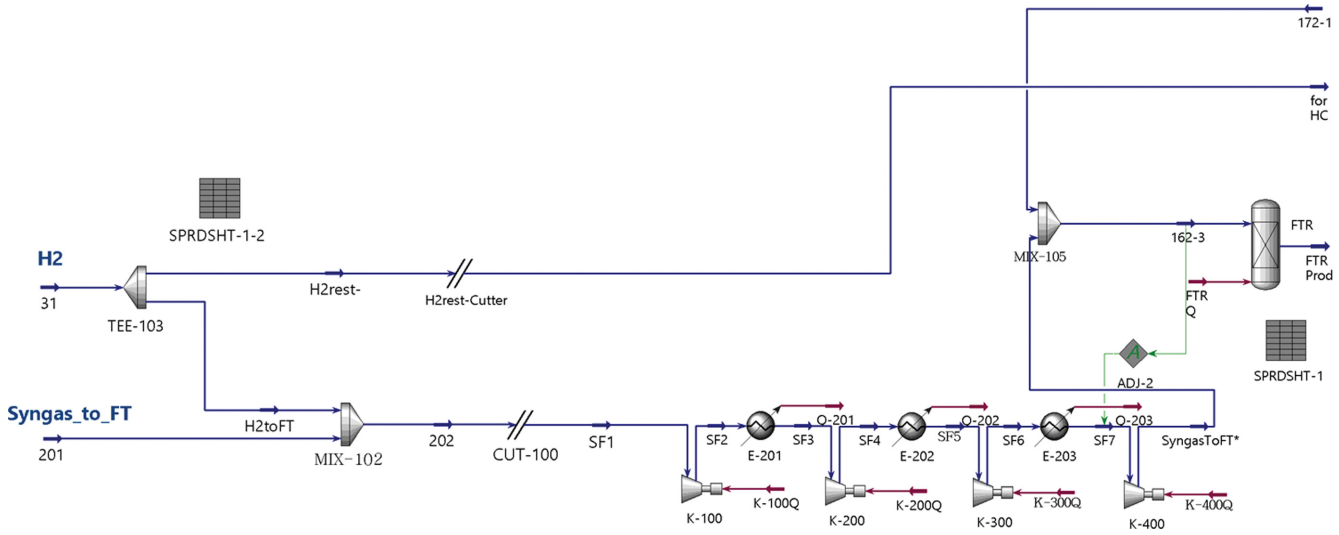

Fig. 4. Fischer-Tropsch unit A from Aspen HYSYS.

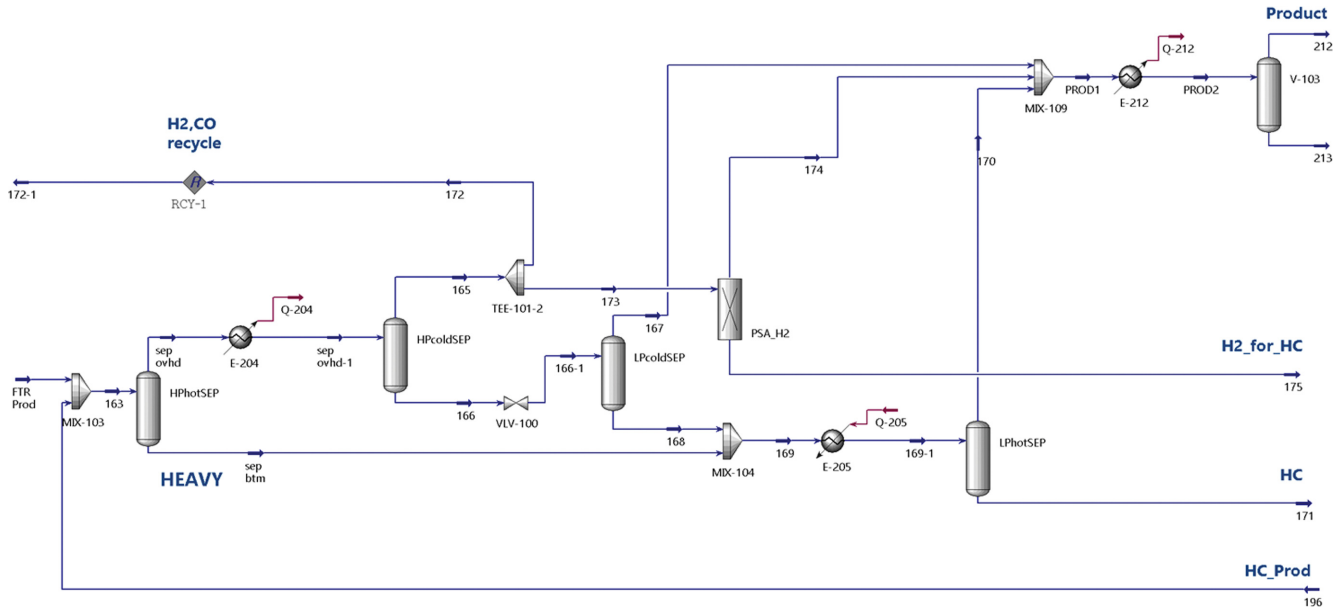

Fig. 5. Fischer-Tropsch unit B from Aspen HYSYS.

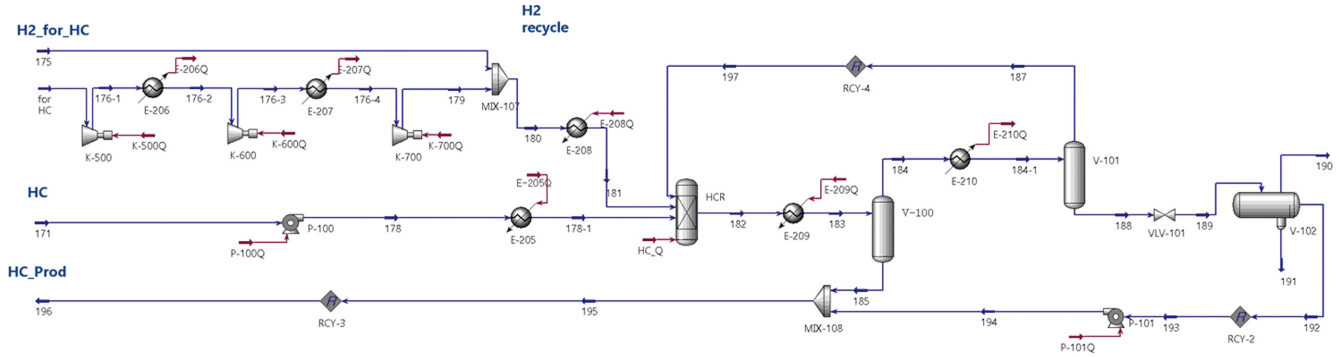

Fig. 6. Hydrocracking unit from Aspen HYSYS.

rials with C20 or less using a hydrocracking process called the upgrading process, as shown in Fig. 6.

The hydrogen required for hydrocracking is sent from the by-product gas treatment and distribution unit to the SOEC and the remaining H_2 is used. The product is separated by passing through the HHPS and CHPS, and the final product is subjected to shear.

The steam turbine cycle was simulated, as shown in Fig. 7. HP steam is produced from waste heat, and electricity is generated through steam turbines and generators. The Rankine cycle is referenced and simulated using the sum of the thermal energies.

The process consists entirely of the steel mill exhaust gas supply chain, HTCE system, F-T process, and hydrocracking process. Waste heat from the hot exhaust gas is used for steam production to provide the energy required for the process. The large amount of CO_2 and H_2 in the exhaust gas is converted into synthetic gas consisting of CO and H_2 via the HTCE system. The generated syngas is subjected to the F-T process, and a hydrocracking process is used to generate liquid products via the F-T process.

PROCESS MODELING AND SETUP FOR ECONOMIC ANALYSIS

1. Process Modeling

1-1. Steel Manufacturing Process

The Korean steel industry currently generates tens of millions of tons of byproduct gas, where representative by-products such as COG, LDG, BFG, and FOG contain high value-added hydrogen and carbon monoxide. The byproduct gas contains a large amount of carbon dioxide. However, the byproduct gas is mainly used as a heat source for power generation because of the problems in separating and utilizing the technical materials, as well as the high cost of refining these materials.

The byproduct gas flow in the steel industry also has high thermal energy, most of which is not recovered but, rather, is released. Because it is challenging to collect information on the thermal energy of byproduct gas in Korea, herein, the "process design" was performed with data from an overseas case study (Table 2).

Table 1. Representative composition and amount of byproduct gas from steel industry [13]

	COG (%)	LDG (%)	BFG (%)	FOG (%)	Total
N_2	7.7	18	49.6	10.6	42
H_2	55.5	2	3.7	11	8.8
CO_2	2.1	12	21.1	46.6	20.8
CO	6.4	68	25.2	30.3	25.5
CH_4	25.2	0	0	1.1	2.3
Misc.	3.1	0	0.4	0.4	0.3
Amount generated (1 million tons/year)	17.2	2.7	55.4	4.5	79.8

Table 2. Heat outputs and energy of the byproduct gases from a steel plant [14]

Byproduct gas	Temperature (°C)	Thermal energy (GJ/t)	Other energy (GJ/t)
COG	649-982	0.17-0.18	0.69
BFG	180-500	0.32-0.82	4.12
LDG	1,600-1,800	0.18-0.21	0.13

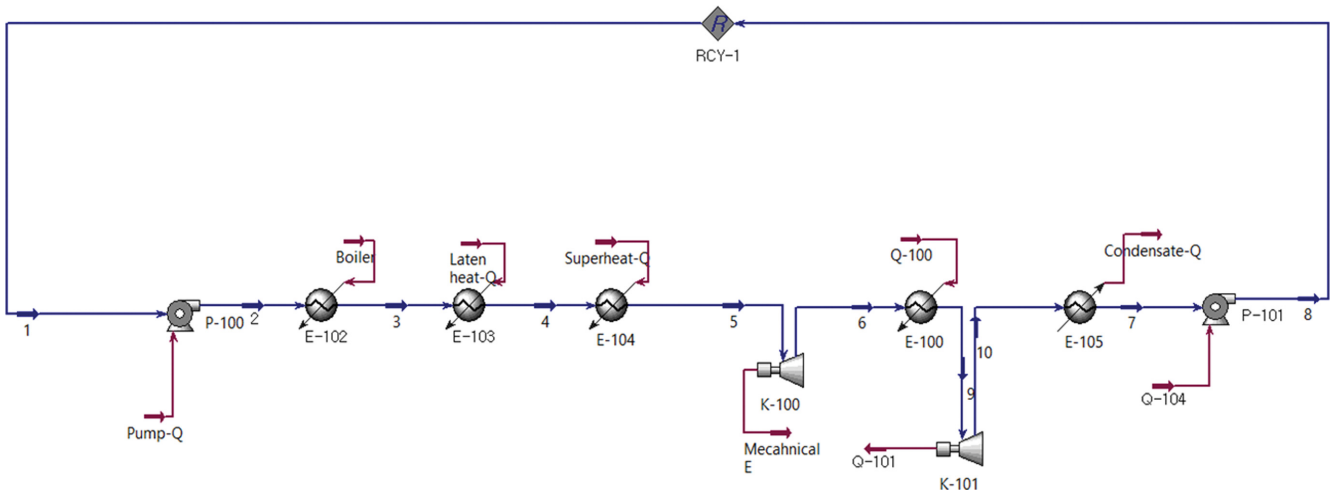

Fig. 7. Steam turbine cycle from Aspen HYSYS.

In this study, the byproduct gas flow rate presented in Table 1 and the thermal energy of the byproduct gas in Table 2 were used to model and analyze the steelworks-linked CO_2 electrolysis and synthetic fuel production process. Among the by-products, COG is refined to control the H_2/CO ratio in the F-T process and is used as a raw material for hydrocracking in the upgrading process. COG is separated and purified to produce syngas for use in the SOEC. In addition, based on the temperature of each byproduct gas stream, the heat-exchange network is designed according to the calorific value required for the SOEC, the F-T process, and upgrading processes.

1-2. Steam/CO_2 Co-electrolysis System: Solid Oxide Electrolysis Cell (SOEC)

The SOEC produces synthetic gas comprising CO and H_2 through electrolysis of CO_2 or H_2O by the reverse reaction of solid oxide fuel cells. As shown in Fig. 8, the SOEC comprises three components ,which are laminated like a sandwich: a cathode, anode, and solid oxide electrolyte. At the SOEC cathode, the feed gas with O sources, such as CO_2 and H_2O, receives electrons via the reactions in Eqs. (1) and (2) and is electrolyzed into CO, H_2, and O ions. The O ions generated in the electrolysis process pass through the anode via the solid oxide electrolyte. Oxygen molecules are generated and discharged, as shown in Eq. (3), and the electrons are recirculated.

$$H_2O+2e^- \rightarrow H_2+O^{2-} \quad (9)$$

$$CO_2+2e^- \rightarrow CO+O^{2-} \quad (10)$$

$$2O^{2-} \rightarrow O_2+2e^- \quad (11)$$

The CO_2/H_2O ratio of the SOEC lead-in flow was approximately 9 : 1, which minimized the flow rate of H_2O to a level that did not cause carbon deposition, thereby improving rate of CO_2 conversion [9].

1-3. Fischer-Tropsch Synthesis (FTS)

The FTS produces various synthetic products via catalytic chemical conversion of syngas. The carbon chain of syngas grows by inserting a methylene group (-CH_2-), where syngas is converted into a hydrocarbon compound. Eq. (12) represents a fundamental reaction in FTS. This reaction generates a large amount of heat; thus, the FTS reaction is exothermic.

$$CO+2\,H_2 \rightarrow -(CH_2)-+H_2O \quad \Delta H^o_{FT}=-165\,kJ/mol \quad (12)$$

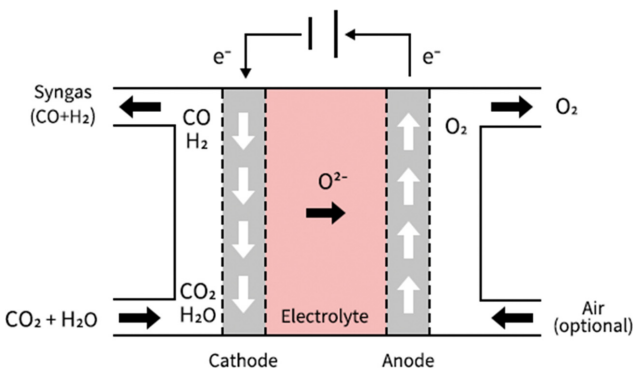

Fig. 8. Principle of solid oxide electrolysis cell (SOEC) for the co-electrolysis of steam/CO_2 to produce syngas and oxygen [9].

Paraffin and olefin products are also generated through the following reactions:

$$nCO+(2n+1)\,H_2 \rightarrow C_nH_{2n+2}+n\,H_2O \quad (13)$$

$$2nCO+(n+1)\,H_2 \rightarrow C_nH_{2n+2}+n\,CO_2 \quad (14)$$

$$nCO+2n\,H_2 \rightarrow CnH_{2n}+n\,H_2O \quad (15)$$

$$2nCO+n\,H_2 \rightarrow C_nH_{2n}+n\,CO_2 \quad (16)$$

$$nCO+2n\,H_2 \rightarrow C_nH_{2n+1}+(n-1)\,H_2O \quad (17)$$

The product range applied to the F-T reaction step in this study was set by considering the above scheme (Eqs. (13)-(17)).

There is a High-Temperature Fischer-Tropsch (HTFT) and a Low-Temperature Fischer-Tropsch (LTFT) in FTS. In this study, the LTFT was used to commercially produce high-quality intermediate distillates using a supported cobalt catalyst supported. The conditions of LTFT are generally 210-250 °C and α-values of 0.88-0.95.

Eqs. (18)-(19) are used to estimate the ASF distribution, as shown in Fig. 9.

$$m_n=(1-\alpha)\,\alpha^{(n-1)} \quad (18)$$

$$\alpha=Rp/(Rp+Rt) \quad (19)$$

where, m_n is the mole fraction of a hydrocarbon with chain length n and α is the growth probability factor.

The α value, a chain growth probability index, was set to 0.9, and the product yield was applied.

The main parameters used in the Aspen HYSYS simulation of the F-T reaction are summarized in Table 3. The temperature and pressure of the reactor inlet feed were adjusted to 485 K and 20 bar, respectively, through a four-stage compression and adjustment function with a compression ratio of 2. The H_2/CO ratio was set to two by adjusting the amount of H_2 supplied to the feed for an appropriate reaction. Initially, Excel was used to estimate the composition distribution of the product, using Eqs. (18) and (19). Once sets of data for the compositions of feeds and products were obtained, they were applied to a yield shift reactor. For reference, the

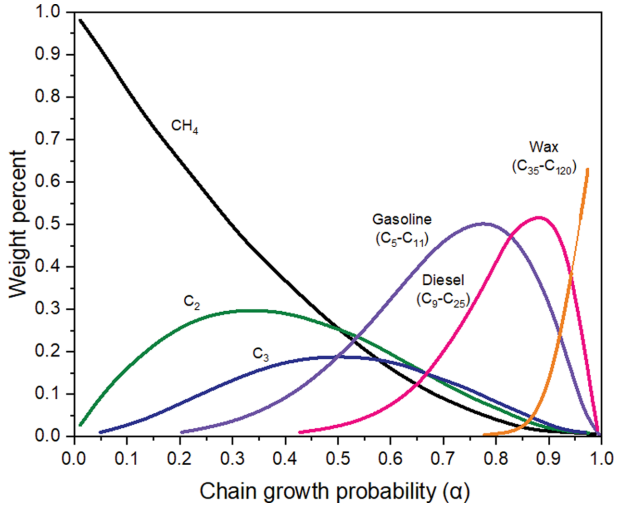

Fig. 9. Anderson-Schulz-Flory (ASF) distribution (α=0.9) [15].

Table 3. Essential parameters for Fischer–Tropsch reaction (FTR)

F-T feed compression		F-T feed		F-T reactor	
Stage	4	Temperature	485 K	H_2 conversion	87.9%
Compression ratio	2.1	Pressure	20 bar	CO conversion	84.6%

Table 4. Activity of Me-HZSM-5 [23]

	Eicosane conversion (wt%)	Paraffin selectivity	Olefin selectivity	Aromatics selectivity	Gaseous products selectivity
Me-HZSM-5	99.99	53.07	1.21	37.27	43.88

Conditions: Temperature: 300 °C and pressure: 20 bar.

H_2 conversion rate was 87.9% and the CO conversion rate was 84.6% [16]. The separation process at the rear end of the reactor was simulated by using separator and splitter operations. Materials with C19 or fewer carbon atoms are sold as products, and materials with C20 or more carbon atoms are sent to the upgrading process for hydrocracking.

1-4. Upgrading Process

In the scenario where a large amount of residual H_2 from the byproduct gas of the steelworks process is utilized in the advanced process, it is expected that the heavy oil produced after the F-T process will be converted into high-value-added light crude. As a progressive step, the oil can optionally be decomposed via hydrogenation. The hydrogenation step is preferred for decomposing F-T wax, which contains a wide-range of carbon atoms. Various types of heavy oils can be decomposed via this process, depending on the catalyst, temperature, and pressure conditions [17]. In the hydrogenation reaction, many benzene rings in heavy oil can be easily decomposed using a catalyst, and unsaturated hydrocarbons can be converted into saturated hydrocarbons to produce high-quality heavy oils. The oils react with coke generated during the decomposition step to produce methane, preventing coke from accumulating in the process.

The kinetics of the hydrogenation-based decomposition step are expressed as follows, based on the reaction rate and the resin material. First, the rate equations for reactions (20)-(24) are as follows [18-22]:

Rate of isomerization and hydrocracking (i=carbon number):

$$r_{isom}(i)=\frac{k_{isom}(i)\times\left(P_n(i)-\frac{P_{iso}(i)}{K_{eq}(i)}\right)}{P_{H_2}(1+\Sigma_{i=1}^{n}P_n(i)\times K_{L,n}(i)+\Sigma_{i=4}^{n}P_{iso}(i)\times K_{L,iso}(i))} \quad (20)$$

$$r_{ck}(i)=\frac{k_{ck}(i)\times P_{iso}(i)}{P_{H_2}(1+\Sigma_{i=1}^{n}P_n(i)\times K_{L,n}(i)+\Sigma_{i=4}^{n}P_{iso}(i)\times K_{L,iso}(i))} \quad (21)$$

Rate of product formation:

$$r_{prod,iso}(i)=\gamma\times\Sigma_{=i+4}^{n}\left(\frac{2}{j-6}\times r_{ck}(i)\right)+\left(\frac{2}{2\times(i+3)-12}\times r_{ck}(i+3)\right) \quad (22)$$

Rate of product formation:

$$r_{prod,n}(i)=(1-\gamma)\times\Sigma_{j=i+4}^{n}\left(\frac{2}{j-6}\times r_{ck}(i)\right) \quad (23)$$

$$r_{prod,n}(i=3)=\Sigma_{j=7}^{n}\left(\frac{2}{2\times j-6}\times r_{ck}(i)\right) \quad (24)$$

The equations for the decomposition of various resins (25)-(30) are as follows:

Normal paraffins:

$$\frac{\partial C_n(3)}{\partial W_{cat}}=r_{prod,n}(3) \quad (25)$$

$$\frac{\partial C_n(i)}{\partial W_{cat}}=r_{prod,n}(i)-r_{isom}(i) \qquad i=4-66 \quad (26)$$

$$\frac{\partial C_n(i)}{\partial W_{cat}}=-r_{isom}(i) \qquad i=66-70 \quad (27)$$

Iso paraffins:

$$\frac{\partial C_{iso}(i)}{\partial W_{cat}}=r_{prod,iso}(i)+r_{isom}(i) \qquad i=4-5 \quad (28)$$

$$\frac{\partial C_{iso}(i)}{\partial W_{cat}}=r_{prod,iso}(i)+r_{isom}(i)-r_{ck}(i) \qquad i=6-67 \quad (29)$$

$$\frac{\partial C_{iso}(i)}{\partial W_{cat}}=r_{isom}(i)-r_{ck}(i) \qquad i=68-70 \quad (30)$$

In the hydrogenation-based decomposition step, Me-HZSM-5, which has a high conversion rate for C20+ species and high selectivity for paraffin-based and gaseous products, was adopted as the catalyst (shown as Table 4). The product compositions were initially estimated based on catalyst information as shown in Table 4, and these obtained sets of data for feed and product compositions were applied into the yield-shift reactor model. The product was produced using a reactor temperature of 300 °C and a pressure of 20 bar. This production process was copied herein [23]. In addition, residual hydrogen was supplied to the hydrogenation-based decomposition reactor through recycling in the subsequent stage. The final product was sent to the shear classification process in upgrading step.

1-5. Utilities

Considering the large scale of piping lines, costs according to the scale of the process, safety of primary explosive substances such as H_2 and CO, the exhaust gas supply network of the entire process, HTCE system, F-T process, and the exhaust gas supply network between the upgrading processes, a steam-based Rankine

Table 5. Power produced from steam turbine supplied with 40 bar superheated steam at 500 °C [24]

Steam pressure (bar)	Saturation temperature (°C)	Steam exhaust temperature (°C)	Shaft work produced (kWh/tons steam)	Power/T_{sat} (kWh/°C)
40	250	500, superheated	0	
30	234	459, superheated	23	1.44
20	212	404, superheated	53	1.40
10	180	309, superheated	98	1.40
5	152	247, superheated	136	1.40
2.25	124	176, superheated	173	1.39
1	100	114, superheated	206	1.37
0.44	78	78, saturated	236	1.37
0.2	60	60, saturated	263	1.38
0.074	40	40, saturated	292	1.39

cycle was utilized as an efficient energy distribution medium.

High pressure steam (250 °C, 40 bar) and low pressure (125 °C, 2.3 bar) steam were used in the process. The temperature and pressure used for steam production are summarized in (Table 5), where the system was supplied with exhaust gas. Steam production using waste heat from the network and HTCE system was optimized.

The steam produced is used for electricity production and direct heat exchange via the turbines. First, low-pressure steam passing through the turbine is condensed through the condenser. The condensed water is pressurized isentropically through a pump [25]. The pressurized water utilizes the waste heat from the steelworks, and the phase change from the liquid phase to the gas phase progresses through heat exchange with the exhaust gas. This steam is eventually used for direct heat exchange and power production by driving a turbine. The energy recovered in the steam cycle was 19.49 MW, and the efficiency was 32.15%.

2. Setup for Economic Analysis

2-1. Capital Expenditure (CAPEX)

The capital expenditure (CAPEX), as listed in Table 6, is calculated based on the installation cost of the equipment used in each process. The installation cost for each equipment was calculated based on Eqs. (31)-(33) [26].

And all equipment costs were calculated according to Eq. (33) based on the Chemical Engineering Plant Cost Index (CEPCI) due to the difference in the published price year [27]. The 2021 CEPCI was taken at 699.7 [28].

$$\text{Equipment installation cost} = \text{purchased equipment cost} \times \text{installation factor} \quad (31)$$

$$\text{Purchased equipment cost} = \text{base cost} \times (\text{new size}/\text{base size})^{\text{Scaling exponent}} \quad (32)$$

$$\text{Cost in Current Year} = \text{Cost in Quoted Year} \times \frac{\text{Curent year cost index (2021)}}{\text{Quote year cost index}} \quad (33)$$

The cost of the SOEC system is $3,424/kW, which was calculated based on the power of the SOEC system (9,653 kW). The balance of the plant (BOP) was set to 66% and was calculated as 66% of the SOEC system. The supplement cost was calculated as 20% of the SOEC system plus BOP.

Additionally, the capital cost of CO_2 PSA is calculated as $1,681,457/yr based on 0.1713 molar fraction of CO_2 in feed with a flowrate of 0.7817 kmol/s [39].

The required equipment for the FT & hydrocracking process and the power generation part was calculated by applying the scaling exponent value and installation factor based on each reference.

Outside battery limit (OSBL) costs are estimated to be 40% of inside battery limit (ISBL) costs, and engineering costs are 10% of the sum of ISBL costs and OSBL costs for larger processes. In the case of SOEC, it is excluded because all costs are included in the balance of plant (BOP) and supplement. The calculated OSBL costs and engineering costs are $83,338,218 and $29,168,376, respectively. At this time, the CAPEX price for all operations was calculated to be $386,673,389.

2-2. Operating Expenditure

The OPEX was calculated based on the power required for each process. The waste heat from the byproduct gas generated at the steelworks was recovered, and a steam turbine cycle was used to replenish the power. In the FT and hydrocracking processes, the heat energy required for the F-T reactor and cooler is directly exchanged. The remaining surplus heat energy is used to produce steam to supplement electric power. The required power includes the power for feed multi-stage compression, pumps, and heaters in the F-T and hydrocracking process. The aforementioned components are listed in Table 7.

Additionally, the operating cost of CO_2 PSA is calculated as $5,334,304/yr based on 0.1713 molar fraction of CO_2 in the feed with a flowrate of 0.7817 kmol/s [39].

After subtracting the electricity produced through steam recycling from the total electricity required for the entire process, there is a shortfall of 11.56 MW of electricity, requiring an external supply. The external electricity was supplied by two providers: Korea Electric Power Corporation or a surplus solar power generation system imported from overseas. If the plant operates for 660 h per month, when the electricity shortfall is supplied by the Korea Electric Power Corporation, the electricity bill will be approximately $843,636 per month based on the exchange rate of 1,196.1 Won per dollar. The energy cost for the overseas surplus solar power generation system was approximately $473,035 per month in 2020 and is expected to cost $190,740 per month in 2050. The electric-

Table 6. Equipment installation cost and reference

Reaction area	Equipment	Base installation cost	Installation cost	Base capacity	Installation factor	Scaling exponent	References
SOEC	SOEC system		$33,051,872	$3,424/kW			[29]
	BOP		$21,814,236	66% of SOEC			[30]
	Supplement		$10,955,143	20% of SOEC plus BOP			[31]
	Pinch heat exchanger	$933,300	$4,681,480		2.47	0.65	[32]
	H_2 PSA1	$2,050,585	$13,610,477	115.99 kmol/hr	3.02	0.60	[33]
	Feed cooler	$63,900	$1,202,583	1,452,000 Btu/hr	3.20	0.70	[34]
FT	Syngas compressor	$11,900,051	$3,024,466	220,009 Btu/hr	2.47	0.8	[2]
	FT synthesis reactor	$10,500,000	$28,626,252	2.52 million scf/h	3.6	0.72	[35]
	FT product HHPS	$1,490,372	$9,035,339	19,791 ACFH	2.05	0.70	[36]
	FT product CHPS	$245,372	$4,625,674	3,011 ACFH	2.15	0.70	[36]
	FT product CLPS	$245,372	$4,615,045	3,011 ACFH	2.15	0.70	[36]
	H_2 PSA2	$2,050,585	$1,854,162	115.99 kmol/hr	3.02	0.5	[33]
	Gas/liquid separator	$245,372	$1,757,504	9,494 ACFH	4.99	0.70	[36]
	FT product cooler	$295,308	$652,443	2,344,968 Btu/hr	3.20	0.70	[34]
	Product cooler	$295,308	$607,948	2,344,968 Btu/hr	3.20	0.70	[34]
HC	HLPS	$1,490,372	$835,230	19,791 ACFH	2.05	0.70	[36]
	H_2 cooler	$63,900	$331,451	1,452,000 Btu/hr	1.52	0.70	[35]
	H_2 compressor	$2,391,777	$639,813	15,322 lb/hr	2.47	0.60	[2]
	Hydrocracking unit:	$30,000,000	$116,487,887	2,250 bpd fd	2.47	0.65	[37]
	HT product HHPS	Included in Hydfocracking unit					
	HT product CHPS	Included in Hydfocracking unit					
	LP HT effluent flash:3 phase	Included in Hydfocracking unit					
	HT pump	Included in Hydfocracking unit					
	LT pump	Included in Hydfocracking unit					
	HC product cooler	Included in Hydfocracking unit					
	HC feed cooler	$88,705	$268,470	395,651 Btu/hr	3.20	0.70	[36]
Power generation	Steam Turbine and generator	$9,500,000	$6,724,545	−42,200 kW	1.80	0.60	[38]
	Fuel storage	$7,405,996	$8,764,775	350 t/day	3.02	0.65	[35]
Total			$274,166,795				

Table 7. Heat energy and electricity requirements for all processes

Total recoverable thermal energy		Required heat energy		Excess thermal energy		Power requirements	
Byproduct gas supply chain	18.9914 MW	F-T and HC	5.9802 MW	Steam production	19.4916 MW	SOEC	9.653 MW
FT&HC	6.4804 MW			Electricity production efficiency	32.15%	FT&HC	5.9875 MW
						H_2 PSA	2.186 MW
Total	25.4718 MW		5.9802 MW		6.2665 MW		17.8265 MW

ity price of Korea Electric Power Corporation was estimated as $6.76/month of contracted electricity and $0.1/kWh of electricity bill as of January 2022. Overseas surplus solar power was calculated as shown in Table 12.

2-3. Business Validity Analysis-discounted Cash Flow Diagram

The discounted cash flow diagram (DCFD) method was used for the business validity analysis. To develop the DCFD, the period of civil engineering, construction, etc., of the initial process was set to three years; the construction cost was 50%, 30%, and 20% in the first, second, and third years, respectively. Excluding the period required for construction, the project period was set to 20 years in total, considering the service life of the equipment. The cash flows of CAPEX and OPEX were calculated as the present value. The social discount rate was set at 4.5% according to Article 50, Paragraph 1 of the Guidelines for the Implementation of Preliminary Validity Surveys in South Korea. Economic analysis of the revolutionary utilization of CO_2 and waste heat from steelworks coupled with synthetic fuel production was thus performed [40].

RESULTS AND DISCUSSION

1. Mass and Energy Balances

1-1. Mass Balances

CO_2 was recovered from BFG, which has a relatively high amount of CO_2, and H_2 was recovered from COG, which has a high amount of H_2 and is used as the feed for the SOEC. LDG has a high proportion of CO, but a relatively small amount is present; therefore, LDG was used only for waste heat recovery. Air and water were used to supply O_2 to the SOEC. The SOEC produced 438 mol of CO and 35 mol of H_2 from 438 mol CO_2 and 35 mol H_2O; the products were then sent to the F-T and hydrocracking process along with the remaining hydrogen from the COG. In all processes, 336.8 tons/day of syngas with a H_2/CO ratio of 2 was used to produce the final products: crude oil 307.6 tons/day and gas 44.32 tons/day. Tables 8-9 show the main flow in all processes. Hydrocarbons with more than 20 carbon atoms were named as C20+.

1-2. Energy Balances

The waste heat that could be utilized from the exhaust gas of the steelworks was used to produce the thermal energy and electric energy required for the process [25]. The thermal efficiency of the process was maximized by optimizing the heat-exchange network based on the exhaust gas supply network and pinch analysis of the HTCE system. The heat-exchange network was optimized using Aspen Energy Analyzer (AEA) after defining the hot/cold stream of the process. With this setup, heat is supplied and recovered internally between the process flows, the heat exchanger arrangement is improved, and the optimum heat-exchange network is designed.

The heat-exchange stream consisted of five hot streams (COG, BFG, LDG, anode out, syngas), three cold streams (air, CO_2, and water), and HP and LP utility streams. The heat-exchange condi-

Table 8. Stream table for SOEC and & waste heat process

Stream No.		COG	BFG	LDG	AIR	H_2O	1	2	3	4	5	7
Vapor fraction		1	1	1	1	0	1	1	1	1	1	1
Temperature	°C	815.5	400	1700	25	25	737.5	801	800	791	682	50
Pressure	bar	1	1	1	1	1	1	1	1	1	705.5	1
Mass flow	ton/day	471.2	1518	73.97	338	18.99	530.7	530.7	530.7	530.7	519.8	1520
H_2	Mol. frac.	0.573	0.037	0.020			0.023	0.109	0.109	0.093		0.037
CO		0.066	0.252	0.680			0.070	0.536	0.536			0.252
CO_2		0.022	0.211	0.120			0.762	0.054	0.054	0.832		0.211
O_2					0.21			0.290	0.290		0.468	
N_2		0.080	0.496	0.180	0.79						0.532	0.496
H_2O						1	0.146	0.010	0.010	0.076		0.004
C1		0.260										
C2												
C3												

Stream No.		8	18	22	26	27	29	30	31	201	210	211
Vapor fraction		1	1	1	1	1	1	1	1	1	1	1
Temperature	°C	50.21	831.9	836.5	135	625.8	50	50	50	135	682	135
Pressure	bar	1	1	1	1	1	1	1	1	1	1	1
Mass flow	ton/day	509.1	18.99	509.1	73.97	338	471.2	2.6	53.68	298.7	519.8	519.8
H_2	Mol. frac.				0.020		0.573	1	1	0.169		
CO					0.680		0.066			0.831		
CO_2		1		1	0.120		0.022					
O_2						0.210					0.468	0.468
N_2					0.180	0.790	0.079				0.532	0.532
H_2O			1									
C1							0.260					
C2												
C3												

Table 9. Stream table for F-T and HC process

Stream No.		162-3	163	165	167	169	172	179	181	182	187	188	196	212	213
Vapor fraction		1	0.795	1	1	0.3461	1	1	0.96	0.44	1	0	0.003	1	0
Temperature	°C	211.9	224.9	30	23.76	171.4	30	316	300	300	40	40	263.8	25	25
Pressure	bar	20	20	20	1	1	20	20	20	20	20	20	20	1	1
Mass flow	ton/day	428.8	590.8	119.7	9.35	461.8	93.36	15.46	162.0	163.7	1.704	37.17	162.0	44.24	306.7
C1	Mol. frac.	0.020	0.101	0.139	0.072	0.006	0.139			0.007	0.021	0.002	0.001	0.182	0.001
C2		0.013	0.074	0.093	0.218	0.010	0.093			0.001	0.003	0.001	0.001	0.158	0.004
C3		0.008	0.051	0.053	0.304	0.023	0.053			0.019	0.028	0.039	0.016	0.137	0.014
C4		0.003	0.034	0.023	0.211	0.048	0.023			0.032	0.020	0.090	0.037	0.101	0.037
C5			0.023	0.007	0.073	0.059	0.007			0.021	0.005	0.064	0.027	0.046	0.060
C6			0.018	0.002	0.021	0.060	0.002			0.020	0.001	0.059	0.027	0.016	0.071
C7			0.017	0.001	0.006	0.060	0.001			0.026	0.001	0.071	0.036	0.005	0.075
C8			0.016	0.001	0.002	0.059				0.033		0.081	0.045	0.002	0.075
C9			0.016			0.058				0.041		0.088	0.056	0.001	0.076
C10			0.016			0.058				0.048		0.089	0.065		0.075
C11			0.015			0.057				0.053		0.085	0.072		0.074
C12			0.015			0.057				0.059		0.080	0.081		0.074
C13			0.014			0.052				0.055		0.063	0.076		0.068
C14			0.013			0.047				0.051		0.047	0.069		0.062
C15			0.012			0.044				0.048		0.037	0.066		0.057
C16			0.011			0.040				0.045		0.029	0.062		0.052
C17			0.010			0.036				0.041		0.021	0.056		0.047
C18			0.009			0.032				0.036		0.015	0.049		0.042
C19			0.008			0.028				0.029		0.010	0.040		0.036
C20+			0.041			0.150			0.045	0.068		0.014	0.094		
CO_2															
N_2															
H_2O															
H_2		0.632	0.297	0.416	0.037	0.009	0.416	1	0.955	0.268	0.926	0.015	0.024	0.023	
CO		0.323	0.192	0.266	0.056	0.007	0.266							0.330	0.001

Table 10. Conditions for heat-exchange stream

	T_{in} (°C)	T_{out} (°C)	Pressure (bar)	Mass flow (kg/h)
COG (hot)	815.5	50	1	19,634.7
BFG (hot)	400	50	1	2,081.3
LDG (hot)	1,700	135	1	3,082.0
Anode out (hot)	682	135	1	21,039.8
Syngas (hot)	800	84.97	1	13,270.8
Air (cold)	25	625.8	1	14,083.6
CO_2 (cold)	50.21	836.5	1	19,327.0
Water (cold)	25	831.9	1	791.2

tions, such as the temperature and pressure of each flow, are listed in Table 10. Heat exchange between hot syngas and cold air, which poses a risk of explosion, was eliminated.

1-3. Optimization of Heat-exchange Network Using Aspen Energy Analyzer

First, a stream worksheet for the process simulated by Aspen HYSYS was imported into AEA. The composite curve used to optimize the heat-exchange network is shown in Fig. 10.

In the general chemical process, ΔT_{min} is usually considered as 10-20 °C [41]. In this research, we used 10 °C as the minimum approach temperature. For reference, this approach temperature can be optimized further to increase the energy efficiency of the process. However, our analysis showed that the change of the minimum approach temperature other than 10 °C does not lead to any further increase in terms of energy efficiency in this case study. Considering the cost index based on the imported heat-exchange network conditions, the optimum ΔT_{min} was determined to be 10 °C. In this process, the utility was specified such that all excess

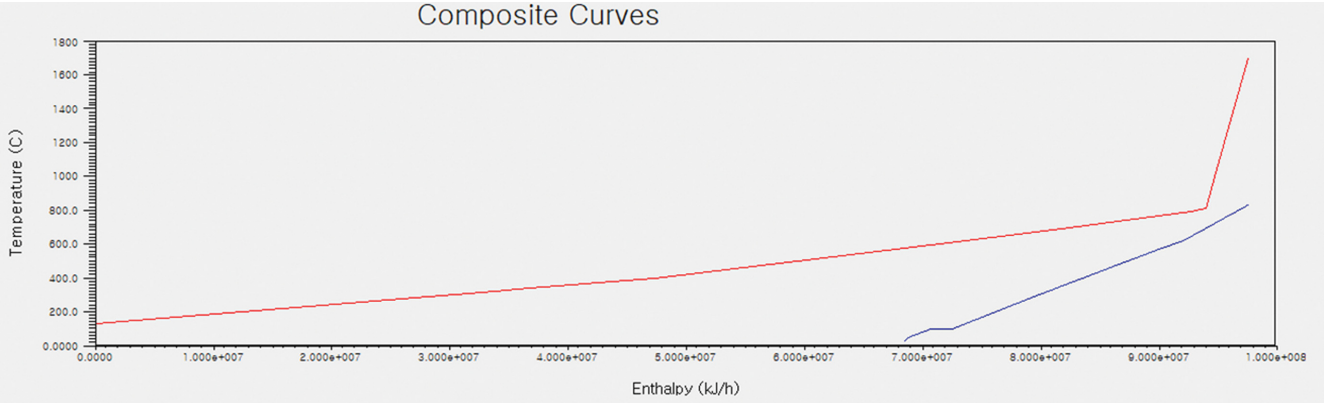

Fig. 10. Composite curve used for heat-exchange network optimization.

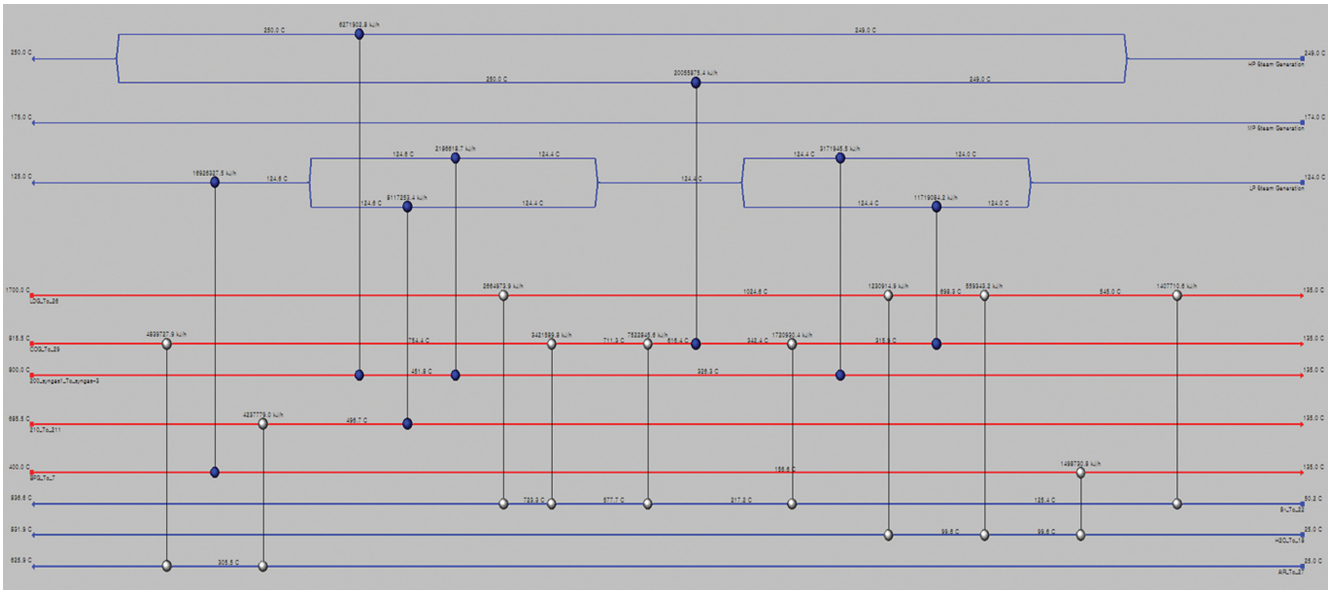

Fig. 11. Grid diagram of the optimized heat-exchange network.

energy of the hot stream for HP, MP, and LP steam production was used under the specified conditions. Cooling below the LP steam heat-exchange temperature was achieved via air cooling. The heat-exchange network with the minimum capital cost was considered. The Grid diagram of the optimized heat-exchange network is shown in Fig. 11.

From optimization of the heat-exchange network, the number of heat exchangers was calculated as 17, the heat-exchange area was estimated to be 15,020.73 m^2, and the capital cost index was calculated as 3,877,709.21. By optimizing the heat-exchange network, 16.4 MW of thermal energy was recovered from the exhaust gas and used for steam production.

2. Economic Analysis

2-1. Income Statement Estimate

The operating profit was calculated using the operating revenue (crude oil, gas sales cost, and carbon emission rights revenue) and the operating cost (electricity charge), and the income statement was estimated. The exchange rate was calculated as 1,196.1 Won/dollar based on the data on January 24, 2022. The income statement was evaluated based on the carbon emission credit revenues of crude oil (78,030 barrels/month), gas (76,890 MMBTU/month), and the carbon dioxide reduction (13,560 tons/month), which were obtained from the process optimization.

2-2. Cash Flow and Present Value Calculation

The integrated co-electrolysis of CO_2 from the steel mill and synthetic fuel production process was considered during the project period of 15 years (2025-2044), excluding the construction year (2022-2024). The present values to which the Korean social discount rate (4.5%) is applied were taken into consideration. When the cash inflow and cash outflow are converted into current weights, they are approximately \$854, and \$478 MM, respectively, and the net present value (NPV) is calculated to be \$376 MM; the profitability index (PI) is 1.79, and the internal rate of return (IRR) is derived as 19.32%. Table 11 and Fig. 12 show the DCF and DCFD. Because PI≥1, this project is deemed appropriate for implementation, where it was confirmed that the payback period is approximately five years, and profits will be generated from 2027.

2-3. Case Study: Utilization of Renewable Energy

Table 11. Discounted cash flow of the integrated process (MM$)

Year	PV	PV_re2020	PV_re2050
2022	−137	−137	−137
2023	−219	−219	−219
2024	−274	−274	−274
2025	−89	−84	−82
2026	−44	−33	−29
2027	0	15	22
2028	42	62	70
2029	82	106	116
2030	121	149	161
2031	157	190	203
2032	193	229	244
2033	226	266	282
2034	258	302	320
2035	289	336	355
2036	319	369	389
2037	347	400	422
2038	374	430	453
2039	400	458	483
2040	424	486	511
2041	448	512	539
2042	471	537	565
2043	492	561	590
2044	513	584	614

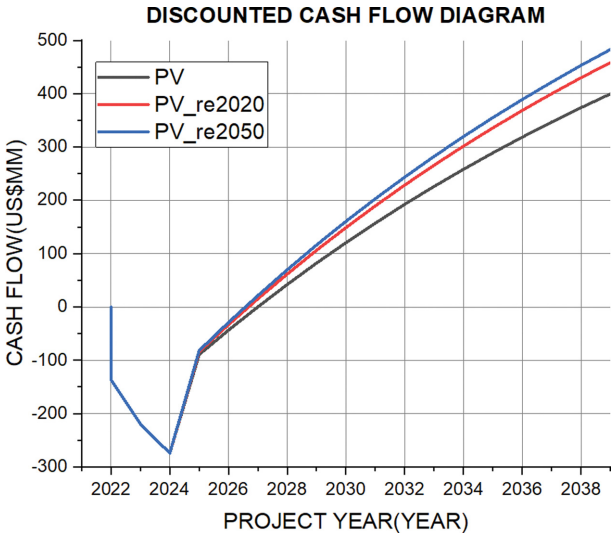

Fig. 12. Discounted cash flow diagram for integrated process.

Table 12. Levelized cost of electricity (LCOE) [42]

Year	2010	2018	2030	2050
Solar PV (USD/kWh)	0.37	0.085	0.08-0.02	0.05-0.01

A case study was conducted by utilizing power from the Korea Electric Power Corporation of 2022 or from new renewable energy (sunlight) of 2020 and 2050 as variables for the power supply; this is the only external inflow energy in the analysis of the integrated CO_2 co-electrolysis and synthetic fuel production process. The electricity rate for solar energy was calculated by applying the 2020 solar production electricity rate and the 2050 forecast value for the surplus electricity supplied by the new renewable energy system imported from overseas [42].

By converting the cash inflow and cash outflow for the case to which the 2020 standard solar electricity rate of $0.062/kWh is applied to the present value, the obtained values are $854 MM and $407 MM respectively, and the net present value (NPV) is $447 MM. The NPV was calculated by applying a PI of 2.10 and an internal rate of return (IRR) of 21.65%. By converting the cash inflow and cash outflow of the case to which the 2050 forecast standard solar electricity rate of $0.025/kWh is applied into the present value, the respective values are $854 MM and $378 MM; the NPV is $477 MM based on a PI of 2.26 and IRR of 22.60%.

CONCLUSION

A process for producing synthetic gas through SOEC-based CO_2 co-electrolysis using byproduct gas from a steel mill in South Korea was developed. The syngas was converted to synthetic fuel through downstream F-T and hydrocracking processes. Economic analysis of the process showed that profits are expected from the sales of carbon emission credits corresponding to 76,890 MMBTU/month and carbon dioxide reduction of 13,560 tons/month, in addition to the production of 78,030 barrel/month of synthetic oil. The recovery of waste heat from the steel mill was maximized by using a pinch technique, maintaining the SOEC operation at high temperatures of up to 900 °C, for example. Furthermore, a portion of the heat was used to produce electricity through the HRSG by utilizing a steam turbine in the SOEC. Two separate cases were considered for filling the electricity shortfall in the SOEC in terms of economic analysis: 1) the Korea Electric Power Corporation and 2) a solar power system from overseas. The results showed that the developed process can produce a profit after five years when the electricity shortfall is filled by the Korea Electric Power Corporation, while the payback period (PBP) would be significantly shortened if electricity is supplied by the solar power system imported from overseas.

ACKNOWLEDGEMENT

This study was funded by the Ministry of Trade, Industry, and Energy (MOTIE) and supported by the Korea Institute of Energy Technology Evaluation and Planning (KETEP), Republic of Korea (Project No. 20182010600400). This work was also supported by Korea Institute for Advancement of Technology (KIAT) grant funded by the Korea Government (MOTIE) (P0008475, Development Program for Smart Digital Engineering Specialist).

DECLARATION OF INTEREST

The authors declare that they have no known competing financial interests or personal relationships that could have influenced the work reported in this study.

REFERENCES

1. L. Holappa, *Metals*, **10**, 1117 (2020).
2. V. Dieterich, A. Buttler, A. Hanel, H. Spliethoff and S. Fendt, *Energy Environ. Sci.*, **13**, 3207 (2020).
3. J. K. Lee, S. Shin, G. J. Kwak, M. K. Lee, I. B. Lee and Y. S. Yoon, *Energy Convers. Manag.*, **224**, 113316 (2020).
4. H. Xi, X. Wu, X. Chen and P. Sha, *Appl. Energy*, **295**, 117069 (2021).
5. R. Gao, C. Zhang, G. Kwak, Y. J. Lee, S. C. Kang and G. Guan, *Energy Convers. Manag.*, **213**, 112819 (2020).
6. Y. Zeng, X. Xiao, J. Li, L, Sun, C. A. Floudas and H. Li, *Energy*, **143**, 881 (2018).
7. K. D. Ras, R. V. D. Vijver, V. V. Galvita, G. B. Marin and K. M. V. Geem, *Curr. Opin. Chem. Eng.*, **26**, 81 (2019).
8. M. Czachor, C. J. Laycock, S. J. W. Carr, J. Maddy, G. Lloyd and A. J. Guwy, *Energy Convers. Manag.*, **225**, 113455 (2020).
9. Q. Fu, C. Mabilat, M. Zahid, A. Brisse and L. Gautier, *Energy Environ. Sci.*, **3**, 1382 (2010).
10. J. E. O'Brien, M. G. McKellar, C. M. Stoots, J. S. Herring and G. L. Hawkes, *Int. J. Hydrog. Energy*, **34**, 4216 (2009).
11. W. L.Becker, R. J. Braun, M. Penev and M. Melain, *Energy*, **47**, 99 (2012).
12. F. Salomone, E. Giglioa, D. Ferrero, M. Santarelli, R. Pirone and S. Bensaid, *Chem. Eng. J.*, **377**, 120233 (2019).
13. J. H. Kim, *NICE (News & Information for Chemical Engineers)*, **36**, 171 (2018).
14. R. Q. Wang, L. Jing, Y. D. Wang and A. P. Roskilly, *J. Clean. Prod.*, **274**, 122997 (2020).
15. M. Martin, *Industrial chemical process analysis and design*, Butterworth-Heinemann, Oxford (2016).
16. T. S. Lee, *Numerical modeling and simulation of fischer-tropsch packed-bed reactor and its thermal management*, Ph. D Thesis, University of Florida (2011).
17. J. W. Ward, *Fuel Process. Technol.*, **35**, 55 (1993).
18. C. Gambaro, V. Calemma, D. Molinari and J. Denayer, *AIChE J.*, **57**, 711 (2011).
19. B. S. Lee, M. J. Park, Y. A. Kim, E. D. Park, J. S. Han, K. E. Jeong, C. U. Kim and S. Y. Jeong, *Korean J. Chem. Eng.*, **31**, 419 (2014).
20. L. Pellegrini, S. Bonomi, S. Gamba, V. Calemma and D. Molinari, *Chem. Eng. Sci.*, **62**, 5013 (2007).
21. G. F. Froment, *Catal. Today*, **1**, 455 (1987).
22. K. Abhinanyu and S. Shishir, *Pet. Coal*, **54**, 59 (2012).
23. J. L. Hodala, J. S. Jung, E. H. Yang, G. H. Hong, Y. S. Noh and D. J. Moon, *Fuel*, **185**, 339 (2016).
24. I. C. Kemp, *Pinch analysis and process integration: a user guide on process integration for the efficient use of energy*, Butterworth-Heinemann, Oxford (2007).
25. S. Y. Im, J. J. Lee, Y. S. Jeon and H. T. Kim, *KSFM*, **19**, 26 (2016).
26. J. Nyári, M. Magdeldin, M. Larmi, M, Järvinen and A. Santasalo-Aarnio, *J. CO_2 Util.*, **39**, 101166 (2020).
27. W. L. Becker, M. Penev and R. J. Braun, *J. Energy Resour. Technol.*, **141**, 021901 (2019).
28. R. Junsittiwate, T. R. Srinophakun and S. Sukpancharoen, *Energy Sustain Dev.*, **66**, 140 (2022).
29. O. Schmidt, A. Gambhir, I. Staffell, A. Hawkes, J. Nelson and S. Few, *Int. J. Hydrog. Energy*, **42**, 30470 (2017).
30. L. Bertuccioli, A. Chan, D. Hart, F. Lehner, B. Madden and E. Standen, Study on Development of Water Electrolysis in the EU, E4tech Sàrl with Element Energy Ltd, Lousanne, Switzerland (2014).
31. J. S. Kim, H. J. Lee, B. R. Lee, J. I. Kim, H. M. Oh, I. B. Lee, Y. S. Yoon and H. K. Lim, *Energy Convers. Manag.*, **250**, 114922 (2021).
32. P. Spath, A. Aden, T. Eggeman, M. Ringer, B. Wallace and J. Jechura, Technical Report, NREL/TP-510-37408 (2005).
33. A. Mivechian and M. Pakizeh, *Korean J. Chem. Eng.*, **30**, 937 (2013).
34. G. Zang, P. Sun, A. A. Elgowainy, A. Bafana and M. Wang, *J. CO_2 Utill.*, **46**, 101459 (2021).
35. R. M. Swanson, A. Platon, J. A. Satrio, R. C. Brown and D. D. Hsu, Technical Report, NREL/TP-6A20-46587 (2010).
36. A. Dutta, A. H. Sahir, E. Tan, D. Humbird, L. J. Snowden-Swan, P. A. Meyer, J. Ross, D. Sexton, R. Yap and J. Lukas, Technical Report, PNNL-23823 (2015).
37. S. B. Jones, C. Valkenburt, C. W. Christie, D. C. Elliott, J. E. Holladay, D. J. Stevens, C. Kinchin and S. Czernik, Technical Report, PNNL-18284 Rev. 1 (2009).
38. R. Davis, L. Tao, E. C. D. Tan, M. J. Biddy, G. T. Scarlata, J. Jacobson, K. Cafferty, J. Ross, J. Lukas, D. Knorr and P. Schoen, Technical Report, NREL/TP-5100-60223 (2013).
39. M. M. Faruque, R. C. Baliban, J. A. Elia and C. A. Floudas, *Ind. Eng. Chem. Res.*, **51**, 15665 (2012).
40. South Korea: General Guidelines for Preliminary Feasibility Study, Article 50 (1), Directive No. 436, April 25, 2019 enacted.
41. L. March, *Introduction to pinch technology*, Targeting House, Gadbrook Park, Northwich, Cheshire, CW9 7UZ, England (1998).
42. International Renewable Energy Agency (IRENA), FUTURE OF SOLAR PHOTOVOLTAIC Deployment, investment, technology, grid integration and socio-economic aspects, A Global Energy Transformation paper (2019).